Geophys. J. Int. (2005) **163,** 956–961 doi: 10.1111/j.1365-246X.2005.02817.x

Banana-doughnut kernels and mantle tomography

Robert D. van der Hilst[1] and Maarten V. de Hoop[1,2]

[1]*Department of Earth, Atmospheric, and Planetary Sciences, Massachusetts Institute of Technology, Cambridge,* MA 02139, *USA. E-mail: hilst@mit.edu*
[2]*Center for Computational and Applied Mathematics, Purdue University, West-Lafayette,* IN 47907, *USA*

Accepted 2005 September 27. Received 2005 September 27; in original form 2005 July 6

SUMMARY

Theoretical analyses suggest that finite-frequency effects should be considered in tomographic inversions of seismic phase 'arrival times' measured with waveform cross correlation at relatively low frequencies. This has led to the development of so-called 'banana-doughnut [sensitivity] kernels'—hereinafter BDKs. Here we address a practical question: has the use of these kernels produced tomographic images of global mantle heterogeneity that are significantly better than those based on ray theory? A simple model comparison suggests that the answer is 'not yet'. The effect of BDKs on both the pattern and the amplitude of mantle wavespeed perturbations appears to be smaller than that of practical (and subjective) considerations (such as the level of damping, the weighting of different data sets, and the choice of data fit) and does not exceed realistic estimates of image uncertainty due to, for instance, errors in the data. By itself, the fact that the better theory has not yet resulted in significant model improvements does not imply that models based on BDKs are incorrect. Deep 'plumes' may very well exist, but the benificial effect of BDKs on the tomographic images (and on 'plume' identification in particular) has been overstated.

Key words: banana–doughnut kernels, global tomography, plumes.

1 INTRODUCTION

The use of 3-D sensitivity kernels in finite frequency tomography has received much attention, both among theoreticians and 'users' of images of mantle structure and, in particular, of 'plumes'. Inspired by the work by Dahlen *et al.*, De Hoop & Van der Hilst (2005a) discussed under which assumptions the so called 'banana doughnut kernels' (BDKs) can be considered reasonable descriptions of the actual finite frequency sensitivity. This prompted a 'Comment' and 'Reply' dialogue between Dahlen & Nolet (2005) and De Hoop & Van der Hilst (2005b). The original version of that exchange also addressed the impact of BDKs on the tomographic images presented by Montelli *et al.* (2004a,b), hereinafter M04a,b, but Dahlen and Nolet (private communication, 2005) requested that we publish this material separately. This is done here.

Theoretical issues aside, it is important to know if BDKs produce better images. De Hoop & Van der Hilst (2005a) noted that 'differences between results of global travel time inversion based either on geometrical ray theory or on finite frequency theory have, so far, been small and—probably—less significant than the effects on the images of uneven spatial and spectral data coverage, data quality, parametrization, and regularization.' We show here the type of observation that motivated their remarks.

We compare models produced with ray theory (that is, high frequency approximation and use of 'ray paths')—hereinafter RT—or with finite frequency theory (that is, with BDKs)—hereinafter FFT; we consider PRI-GJI-RT, a model due to M04a (based on long period *P* and *PP-P* data measured by Bolton & Masters (2001) and inverted using RT); PRI-GJI-FFT, due to M04a (same data but inverted using BDKs); PRI-SCI-FFT, due to M04b (combination of the long period data, backprojected using BDKs, and short-period *P* and *pP* data due to Engdahl *et al.* (1998), hereinafter EHB, backprojected used RT); and MIT-P05 (Van der Hilst, Li & Kárason, in preparation). The latter is based on a data set that is comparable to that used by M04b, with the notable exception that we did not use long period *P* data and that we used a larger portion of the EHB *P* and *pP* data.[1]

Here we use tomographic images to illustrate certain aspects of the models that are relevant to the discussion of the effect of BDKs on global tomography. Comprehensive model comparisons and detailed discussions of mantle structure are not the subject of this research note.

2 EFFECTS OF BDKS ON IMAGES OF 'SLABS' AND 'PLUMES'

Fig. 1 depicts slabs of subducted lithosphere below South America according to PRI-GJI-RT (top left), PRI-GJI-FFT (top right), PRI-

[1]We also use 3D kernels to combine long period *PP-P* (and $P_{\mathrm{diff}} - PKP$) with the short period *P* and *pP* data Kárason & Van der Hilst (2001) and Kárason (2002), but we found that with the parametrization and damping used 'fat rays' and BDK-like kernels produced similar images. We use an irregular grid parametrization and we account for the effect of strong crustal heterogeneity on the images.

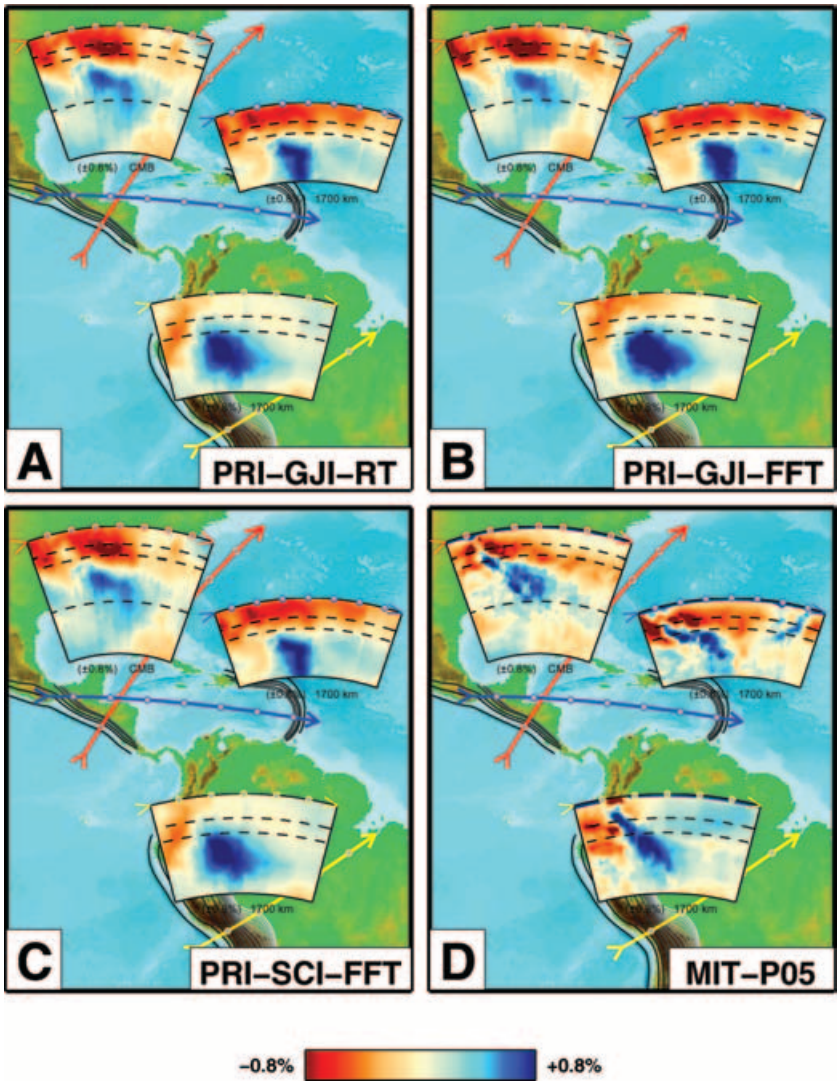

Figure 1. Mantle structure beneath the major convergent margins of Central and South America according to (a) PRI-GJI-RT (M04a); (b) PRI-GJI-FFT (M04a); (c) PRI-SCI-FFT (M04b), and (d) MIT-P05 (Van der Hilst et al., in preparation). Lateral variations in *P*-wavespeed are shown with respect to a 1-D reference model. The color scale is the same for all models, but the amplitude of the anomalies in the models by M04a,b is up to 50 per cent larger than in MIT-P05 so that some color saturation occurs. In each panel, the top-left section extends from Earth's surface to the core mantle boundary (CMB); the middle and lower sections depict wavespeed variations from the surface to 1700 km depth. The large, eastward dipping structures of faster than average *P*-wavespeed (blue) are interpretated as the images of slabs of subducted oceanic lithosphere associated with the ancient Farallon plate; the westward dipping structure in the upper mantle that is visible in middle section of panel D represents the subduction of the Atlantic sea floor beneath the Lesser Antilles. For reference, dashed lines are drawn at 410, 660, and 1700 km depth. Based on the remarkable similarities between the PRI-GJI-RT, PRI-GJI-FFT, and PRI-SCI-FFT images we attribute the differences between MIT-P05 and PRI-FFT not to the use of BDKs but to differences in parametrization, regularization, and data misfit criterion.

SCI-FFT (bottom left), and MIT-P05 (bottom right). It appears that the PRI RT and FFT images are very similar to each other, but they all lack the upper mantle structures revealed in MIT-P05, and the lower mantle structures appear more blurred. Specifically, visual inspection of Figs 1(a)–(c) suggests that neither the use of BDKs nor M04b's use of short-period EHB data has resulted in a significant increase in ability to image these structures. Similar observations can be made for other subduction systems. The apparent inability to resolve these densely sampled features is surprising and may have several explanations. The long period data may not contain sufficient information about the length scales pertinent to upper mantle slab structures. This is not very likely, however. Besides, the short period EHB data (used in PRI-SCI-FFT) do not bring out more detailed structure either (even though Fig. 1(d) indicates that they should be able to do so). Alternatively, the model parametrization and regularization (damping) used by M04a,b may not allow better resolution of such structures. But then, what about 'plumes'? It is also possible that data (processing) errors degrade the imaging of upper mantle structure regardless of the type of wave propagation theory used. Such a problem is not easily exposed by (checkerboard) resolution tests with synthetic data.

Fig. 2 depicts 'plume' structures in the shallow (top) and the deep mantle (bottom) according to PRI-GJI-RT (left column), PRI-GJI-FFT (middle), and PRI-SCI-FFT (right). Small is in the eye of the beholder, and we invite the readers to judge for themselves the significance of the differences, but the similarity of Figs 2(a)–(f) suggests that plume-like structures (at least the ones shown here) are imaged equally well by RT and FFT.

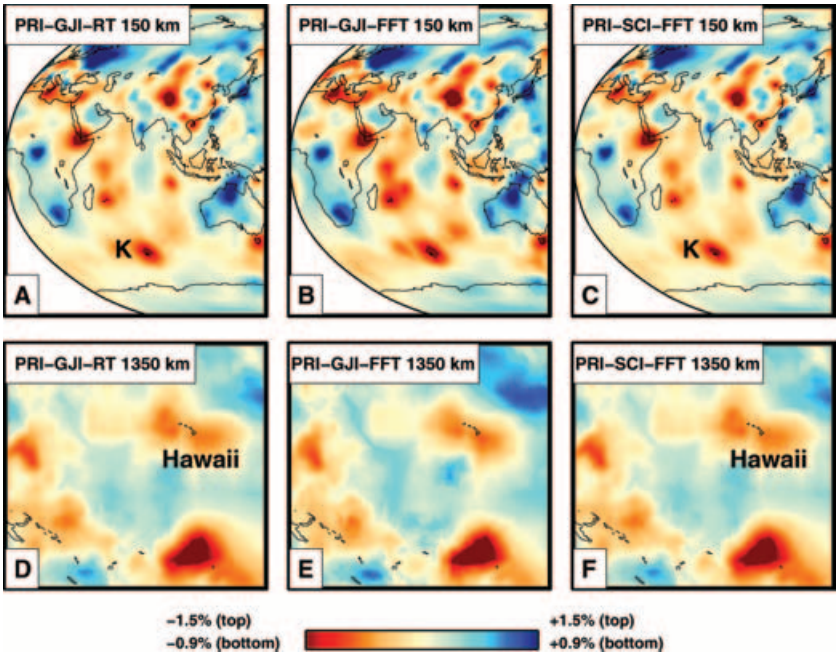

Figure 2. Lateral variation in *P*-wave speed at 150 km depth beneath the Indian Ocean (*K* is Kerguelen) and at 1350 km depth beneath the Pacific according to the models by Montelli *et al.* (2004a,b). Left: result according to PRI-GJI-RT (M04a). Middle: result according to PRI-GJI-FFT (M04a). Right: result according to PRI-SCI-FFT (M04b). The color scales are the same. We leave it to the reader to assess the differences between these RT and FFT results.

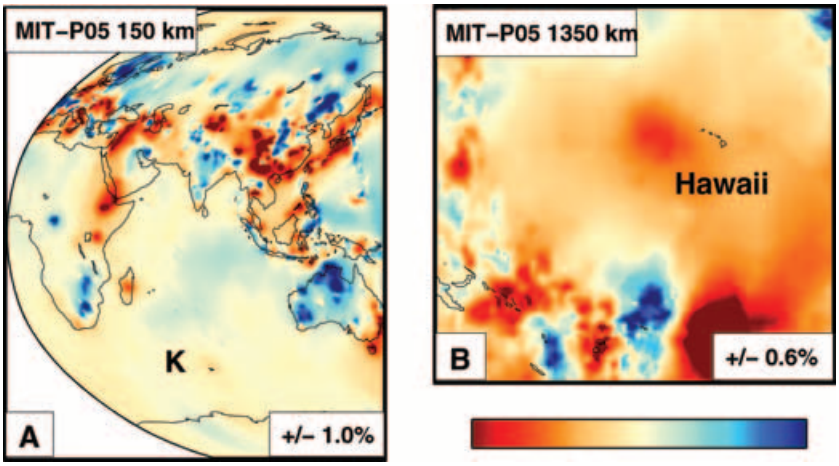

Figure 3. Lateral variation in *P*-wavespeed according to MIT-P05 for the regions and depths used in Fig. 2. We note that the *PP-P* used in our inversions have reduced sensitivity to shallow structure beneath sources and receivers and may, thus, not see all plume-like structures depicted in Figs 2(a)–(c). See also Fig. 4. We note that regularization and the irregular grid combine to produce spatial variations in model smoothness.

For comparison, Fig. 3 depicts the lateral variation in *P*-wavespeed according to MIT-P05. A detailed model comparison is beyond the scope of this note, but there are several observations worth mentioning. First, there are significant differences in amplitude, which can be attributed to different choices of parametrization, damping, and data fit criterion. Second, plume-like structures in the Indian Ocean are absent in Fig. 3(a) (see below). Third, MIT-P05 also reveals low velocity anomalies beneath Hawaii and the southwestern Pacific (Fig. 3b). This can perhaps be used in support of M04b's interpretation in terms of deep mantle plumes, but MIT-P05 reveals only part of the double anomaly that is visible in the PRI models (Figs 2d–f).

By itself, Fig. 3(a) does not demonstrate that 'plumes' do not exist in the upper mantle beneath the Indian Ocean: it is possible that such anomalies cannot be resoved by the data used to construct MIT-P05. For instance, owing to the differential nature of the sensitivity kernels of long period *PP-P* data, the sensitivity to shallow structure beneath sources and receivers is strongly reduced. We have evaluated the resolving power of our tomographic method specifically for the structures discussed here by calculating synthetic data from one of the Princeton models (PRI-GJI-FFT, center column of Fig. 2) and inverting them in the same way as we did to obtain MIT-P05. The result is shown in Fig. 4. While not all of the conspicuous slow anomalies depicted in the PRI models can be resolved,

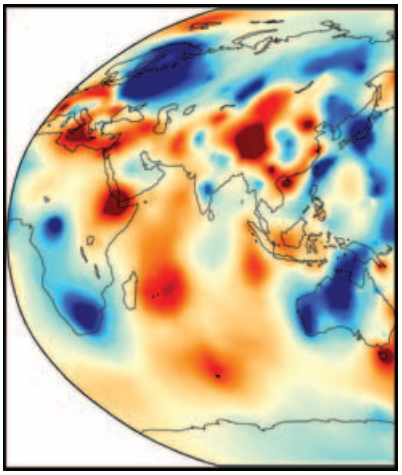

Figure 4. Result of tomographic inversion of synthetic data calculated from one of the PRI models (PRI-GJI-FFT). We calculated synthetic data by multiplying the sensitivity matrix used to construct MIT-P05 with model PRI-GJI-FFT; these data were then inverted in the same way as used to obtain MIT-P05. No noise was added to the data. Comparison with the input model (Fig. 2b) shows that, in general, the recovery of the input model is very good (see, for instance, structure beneath continental Asia), but discrepancies arise in regions were our data coverage is sparser (see Fig. 5c). In particular, our tomography can 'see' most but not all of the conspicuous slow anomalies in the shallow mantle beneath the Indian Ocean.

our data would be able to detect most of them. This indicates that their absence in Fig. 3(a) cannot be explained by lack of resolution alone.

It is, therefore, unlikely that the difference between the MIT and PRI models is due to resolution problems or to the use of a particular wave propagation theory; rather, it may result from M04a,b's use of the long-period *P* data (which, we recall, were not used in our inversions). Fig. 5 suggests that, for this geographical region, (i) the plume signatures show up only below the ocean island stations that contribute to the set of long period *P* data and that (ii) at 150 km depth the image of these 'plumes' (left) is virtually the same as at 450 km depth (middle). This suggests that at least for these upper mantle 'plumes' the use of the long-period *P* data combined with preferred sampling along steep rays (or BDKs) in poorly sampled regions is a concern.

3 EFFECT ON THE AMPLITUDE OF IMAGED MANTLE WAVESPEED PERTURBATIONS

Visual inspection of the examples given above suggests that both the spatial pattern and the amplitude of wavespeed variations in the RT and FFT models are remarkably similar. To shed further light on this, we compare the actual grid values for the different models.

Following M04a, we first consider histograms of wavespeed ratios. Fig. 6(a) shows that for 1350 km depth the ratio of wavespeed variations in PRI-GJI-FFT and PRI-GJI-RT (that is, $\delta c_{\mathrm{GJI-FF}}/\delta c_{\mathrm{GJI-RT}}$) follows a normal distribution with a mean of $\sim$1, which suggests that in most locations the amplitude of the wavespeed anomalies is not substantially influenced by the use of BDKs. Interestingly, Fig. 6(b) shows that in most locations PRI-SCI-FF yields smaller amplitudes than PRI-GJI-RT; this may reflect a difference in data fit ($\chi 2$ value) used. In their analysis, M04a used only anomalies significantly larger than zero ($|\delta c/c| > 0.2$ per cent). The average wavespeed ratio inferred from this type of histogram (Fig. 6c) is significantly larger than 1. Indeed, M04a report 1.5 for the lowermost mantle and 1.3 near Earth's surface (hence an amplitude increase of 50 per cent and 30 per cent, respectively). However, these apparent amplifications are an artifact of the (arbitrary) omission of small values. In agreement with Fig. 6(a), the mode of $\sim$1 suggests that $\delta c_{\mathrm{FF}} \sim \delta c_{\mathrm{RT}}$ in all examples shown in M04a.

We also evaluate the relative behavior of wavespeed anomalies with scatter plots (Figs 6d–f); in these plots, the slope is a measure for the ratio of the anomaly amplitudes in the models considered. We illustrate this for wavespeed anomalies near 1350 km depth, but analysis of such diagrams for all depths suggest that (within realistic error): (i) the anomalies are generally well correlated; (ii) the slopes are significantly less than 1.5 (and 1.3); (iii) the ratio of $\delta c_{\mathrm{SCI-FFT}}$ and $\delta c_{\mathrm{GJI-RT}}$ is not significantly different from one (Fig. 6d); (iv) the amplitude differences between PRI-GJI-FF and PRI-SCI-FF are comparable to or larger than the amplitude differences between PRI-GJI-FF and PRI-GJI-RT (Figs 6e and f), suggesting that other effects (including data weights and choice of χ2-fit) exceed that of the use of BDKs; (v) large ratios (for instance, of the order of the 1.5 mentioned in M04a) do occur, but only for the small (and presumably poorly resolved) wavespeed anomalies.

We thus find that to large depths the FFT and RT anomalies are statistically similar; a discrepancy becomes apparent in the deep mantle but may not exceed 20 per cent.

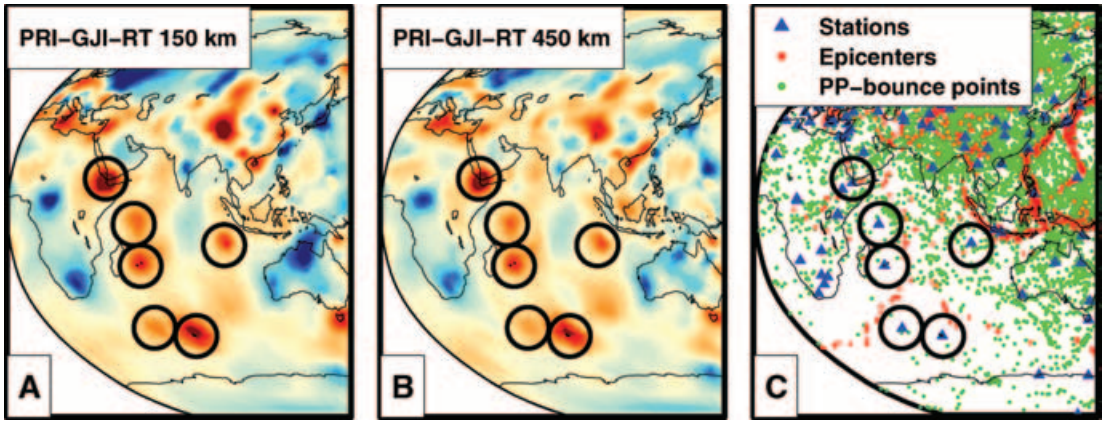

Figure 5. *P*-wave speed at 150 km (left) and 450 km depth (middle) beneath the Indian Ocean according to model PRI-GJI-FFT. Note the similarities between them. The geographical distribution of sources (red dots), receivers (blue dots), and the *PP* bounce points (green dots) is depicted on the right. The *PP* bounce point distribution is sparse in much of the Indian Ocean.

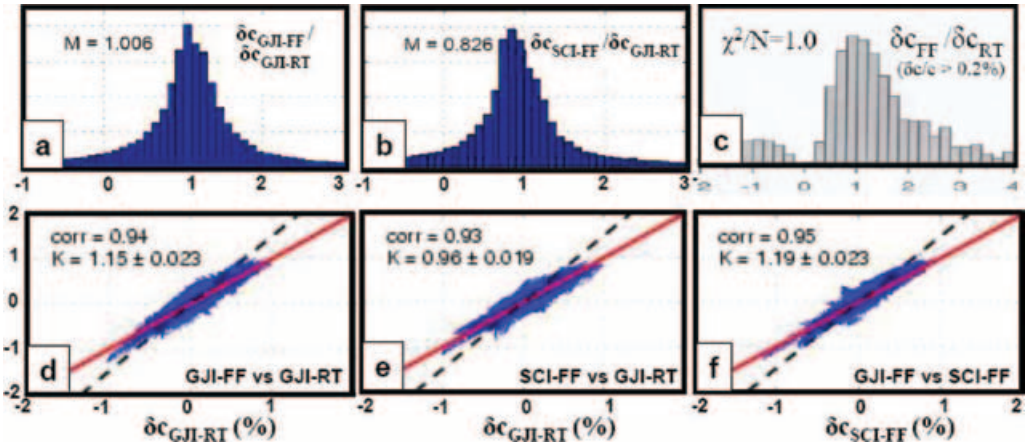

Figure 6. Comparison of wavespeed perturbations δc inferred from FFT and RT inversions by means of histograms and scatter plots. We use $\delta c_{\mathrm{GJI-FF}}$, $\delta c_{\mathrm{GJI-RT}}$, and $\delta c_{\mathrm{SCI-FF}}$ to denote the relative variation in wavespeed according to the PRI-GJI-FFT, PRI-GJI-RT, and PRI-SCI-FFT models, respectively. Unless noted otherwise, we compare the models at a depth of 1350 km in the mantle. (a) histogram of $\delta c_{\mathrm{GJI-FF}}/\delta c_{\mathrm{GJI-RT}}$ (the average value of this distribution is $\sim$1); (b) histogram of $\delta c_{\mathrm{SCI-FF}}/\delta c_{\mathrm{GJI-RT}}$ (the average ratio is $\sim$0.83); (c) histogram of $\delta c_{\mathrm{FF}}/\delta c_{\mathrm{RT}}$ for a depth of 1450 km, for values $|\delta c/c|$ larger than 0.2 per cent, and for models with $\chi^2/N = 1.0$ (after fig. 13 of M04a) (according to M04a the mean of this distribution is around 1.7). The low count near zero, the skewness of the main lobe, and the large averages all result from omitting low values of $|\delta c/c|$ from the analysis. (d) Scatter plot of $\delta c_{\mathrm{GJI-FF}}$ vs. $\delta c_{\mathrm{GJI-RT}}$: the correlation coefficient, R, is 0.94; the slope (from bi-variant regression) is 1.15, with an uncertainty of 0.023 (based on an assumed error in $\delta c/c$ of 0.2 per cent); (e,f) Same for $\delta c_{\mathrm{SCI-FF}}$ vs. $\delta c_{\mathrm{GJI-RT}}$ ($R = 0.93$, slope $= 0.96$) and $\delta c_{\mathrm{GJI-FF}}$ vs. $\delta c_{\mathrm{SCI-RT}}$ ($R = 0.95$, slope $= 1.19$), respectively. The dashed line (slope of 1.5) would be consistent with a $\sim$50 per cent amplitude increase.

4 DISCUSSION AND CONCLUDING REMARKS

As regards the effect of BDKs on the tomographic images, the model comparisons presented here suggest that (i) RT inversions can produce results that are similar to that of FFT inversions with BDKs, and that (ii) amplitude differences between the two FFT models considered here (PRI-GJI-FFT, PRI-SCI-FFT) can be larger than between RT and FFT models (PRI-GJI-RT, PRI-SCI-FFT). The largest differences occur in the lowermost mantle, but even here an increase by 20 per cent of actual anomaly values that are of the order of 0.5–1.0 per cent hardly exceeds realistic measures of amplitude uncertainty.

It is unlikely that the small differences that do occur between the RT and FFT images are resolved by the travel-time data used; indeed, their significance should be questioned in view of the (larger) effects of data error and practical (and subjective) considerations such as the level and type of regularization, the weighting of different data sets, and the choice of data fit (such as the value of $\chi 2$). Similar conclusions are drawn by Trampert & Spetzler (2005) for surface wave tomography. M04a use *Occam's razor* to select 'simple' models, but another perception of 'simple' may yield different amplitudes. Furthermore, in the absence of precise knowledge about data error the $\chi 2$-criterion is difficult to implement objectively. On the one hand, for the $\chi 2$ calculation M04a assume data errors well below 1 s. On the other hand, the long-period P data have an off-set of $\sim$5 s compared to their other data sets; This offset was subtracted from the data but its origin is not well known. With such large intrinsic uncertainties the $\chi 2$–criterion is no less subjective than regularization.

Of course, the similarity of the RT and FFT models does not mean that the tomographic models are incorrect. It is—in our view—not satisfactory, however, that much confidence is placed in the images of elusive 'plumes' while rather uncontroversial structures such as subducted slabs (which, for several reasons, should be easier to image) are surprisingly poorly resolved. Furthermore, the illustrations presented here may inspire a re-assessment of some shallow structures labeled as plumes. Such an exercise may reinforce the interpretations by Montelli *et al.* (2004b), but some revision may be necessary.

NOTE ADDED TO PROOF

It was recently brought to our attention that the PRI models shown here were affected by an error in crust correction (Guust Nolet, private communication, 2005). At the time of finalizing this manuscript the implications of this error were not yet known. It may explain some of the problems with upper mantle slab and plume structures exposed here. However, barring exceptional circumstances, this would not explain the observed similarity of the RT and FFT images and will thus not invalidate our conclusion that the effect of BDKs on the images presented in M04b has been overstated.

ACKNOWLEDGMENTS

We thank Raffaella Montelli and Guust Nolet (Princeton University) for making their models available. Discussions with Bradford Hager (MIT) and Richard O'Connell (Harvard) helped us improve the manuscript. We thank Chang Li (MIT) for preparing material for the figures. Thoughtful reviews by Adam Dziewonski and Barbara Romanowicz helped improve the manuscript. Our research is supported by the NSF grant EAR-0409816 and a Dutch National Science Foundation grant (NWO:VICI 865.03.007) for Innovative Research.

REFERENCES

Bolton, H. & Masters, G., 2001. Travel times of P and S from the global digital seismic networks: Implications for the relative variation of P and S velocity in the mantle, *J. geophys. Res.,* **106**(B7), 13 527–13 540.

Dahlen, F. & Nolet, G., 2005. Comment on 'On sensitivity kernels for wave-equation transmission tomography' by de Hoop and van der Hilst, *Geophys. J. Int.,* **163,** 949–951.

Dahlen, F., Hung, S.-H. & Nolet, G., 2000. Fréchet kernels for finite-frequency traveltimes–I. Theory, *Geophys. J. Int.,* **141,** 157–174.

De Hoop, M. & Van der Hilst, R., 2005a. On sensitivity kernels for 'wave-equation' tomography, *Geophys. J. Int.,* **160,** DOI: 10.1111/j.1365–246X.2004.02509.

De Hoop, M. & Van der Hilst, R., 2005b. Reply to comment by F. A. Dahlen and G. Nolet on 'On sensitivity kernels for 'wave-equation' transmission tomography', *Geophys. J. Int.,* **163,** 952–955.

Engdahl, E., Van der Hilst, R. & Buland, R., 1998. Global teleseismic earthquake relocation from improved travel times and procedures for depth determination, *Bulletin Seismological Society of America,* **88,** 722–743.

Kárason, H., 2002. Constraints on mantle convection from seismic tomography and flow modeling, *PhD thesis*, Massachusetts Institute of Technology.

Kárason, H. & Van der Hilst, R., 2001. Tomographic imaging of the lowermost mantle with differential times of refracted and diffracted core phases (pkp, pdiff), *J. geophys. Res.,* **106,** 6569–6588.

Montelli, R., Nolet, G., Dahlen, F., Masters, G., Engdahl, E. & Hung, S.-H., 2004a. Global P and PP travel time tomography: rays vs. waves, *Geophys. J. Int.,* **158,** 637–654.

Montelli, R., Nolet, G., Dahlen, F., Masters, G., Engdahl, E. & Hung, S.-H., 2004b. Finite-frequency tomography reveals a variety of plumes in the mantle, *Science,* **303,** 338–343.

Trampert, J. & Spetzler, J., 2005. Surface wave tomography: finite frequency effects lost in the null space, *Geophys. J. Int.,* in press.